# PHOTOEMISSION WITHIN AND BEYOND THE ONE-STEP MODEL

**WOLFGANG SCHATTKE**

Institut für Theoretische Physik, Christian-Albrechts-Universität Kiel, Physikzentrum, Leibnizstraße 15, D-24098 Kiel, Germany



## Abstract

Photoemission in the vacuum ultraviolet photon regime has proved to be an effective tool for the investigation of valence band surface electronic structure. The interpretation cannot be exclusively confined to the valence bands but has to consider cross sections with realistic final states consistently designed within the one-step model. Therefore especially in the surface sensitive photoemission, several effects hide the final goal of deducing the energetic and wavefunction structure together with microscopic potential parameters through a convincing agreement of calculated with measured spectra. The final states band structure is much less well understood than the valence band structure under consideration. The optical potential, which controls the surface sensitivity through the underlying damping mechanisms, widely relies on empirical assumptions. Furthermore, the photon field is not only strongly influenced but in the vicinity of the plasma frequency also deteriorated by the electronic response. In view of high resolution spectroscopy the accuracy of the data interpretation is affected, and in fact, band-mapping methods are no longer valid. Examples of recent calculations to account for these effects are reviewed.

## Acronyms

| | |
|---|---|
| DOS | Density of states |
| EDC | Energy distribution curves |
| LCAO | Linear combination of atomic orbitals |
| LEED | Low energy electron diffraction |
| STM | Scanning tunnelling microscope |
| 2D-DOS | Two-dimensionally resolved density of states |

## 1. Introduction

Despite the long tradition, solid state photoemission still continuously experiences new impulses from developments of the experimental equipment and progress in theoretical support. For example, remarkable achievements further accompany the subject of spin dependent photoemission. Being excellently confirmed by experiment theory predicted linear spin polarization on the basis of spin-orbit coupling between states of different orbital symmetry with the consequence of a valence band magnetic linear dichroism. [1] Even for nonmagnetic systems the circular dichroism has proven to be a powerful tool, as e.g. in the investigation of adsorbates. [2] The current design of high resolution detectors of angle resolved photoemission is related to the demand of explaining minute structures as they arise in theoretical investigations on the correlation in high temperature superconductors, or even in surface structures of simple semiconductors. Apart from this development the simultaneous full screen acceptance of the whole emission cone has undergone a revival [3, 4, 5], additionally supported by a new construction of a specifically adapted detector. [6] The roots are localized at the photoelectron diffraction and holography where the link between geometric and electronic properties added complementary understanding of the surface structure. [7] The investigation of the valence-band structure offers to this technique a wide field of application, and has become feasible to theoretical calculation. [8]

Basically, the understanding of the electronic structure of solids and solid surfaces depends on the quality of the photoemission results. Therefore, a steady improvement and a growing amount of data will be necessary to put the actual ab-initio results of electronic structure calculations into a physically realistic context. The knowledge of the electronic energy spectrum is fundamental to many equilibrium and transport properties and thereby photoemission deserves high interest from basic research as well as from technical application. The interplay between band structure calculation and photoemission measurement is controlled by the interpretation schemes to extract the information about the electronic states and their energies from the spectra. There are a lot of more or less heuristic methods which allow a quick access to a part of the physical content in the experimental data. However, all of them lack the accuracy required if the actual high quality of measurement and the actual state of the art of ab-initio calculations should make sense. As in many other techniques the spectra cannot be formally inverted to yield the electronic structure but have to be brought to convergence with theory by trial and error procedures. The clue in the case of photoemission is the so called one-step model, which seems to be a great name for the simple golden rule formula used in calculating cross-sections. But firstly, it has to be contrasted with the three-step model where in a crude way the electron excitation, the transport within the solid, and the escape through the surface into the vacuum are treated as separate incoherent steps. Dealing with good surfaces and moderate temperatures nothing justifies a statistical decomposition of a unique quantummechanical process. Secondly, the adequacy of the one-step model can be based on the safe grounds of general many-body Green function theory. Thirdly, this model has been established long time ago and has proven its reliability and convenience many times. In its simplest version the golden rule formula contains the matrix elements between the initial bound states and the scattering solutions of the same hamiltonian for the dipole operator of the electromagnetic field, and the delta function for energy conservation. The numerical evaluation of that formula yields the photocurrent at the detector which has to be compared with the experimental value. As even ab-initio electronic structure calculations are not free of parameters, one can only minimize the disagreement between experiment and theory in choosing the available quantities appropriately. Here, for the aim of band-structure determinations, we consider emissions from valence states into low energy conduction states as covered by the vacuum ultraviolet photon regime. There may be various approximations in the evaluation of the wavefunctions according to the specific intentions. In the best case one uses a selfconsistently constructed one particle potential adapted to the real surface. Bloch states or equivalently the Green functions for the valence band part as well as the scattering states for the conduction bands are calculated. The latter are equivalent to the time inverse states of a low energy electron diffraction (LEED) system representing the final states accepted by the photoemission detector. The transfer of these ideas into a working numerical program is far from being trivial and has been first accomplished in a closed form by neglecting relativistic effects and choosing muffin-tin potentials obtained from atomic calculations. Since that time a lot of improvements have been achieved finally covering the above mentioned requirements. However, this does not guarantee that the agreement with experiment is splendid. Especially, semiconductors with their reconstructed troublesome surfaces still represent a challenge to theoretical photoemission. [9, 10]

The foregoing considerations of the one-step model apply to the one-particle picture of electrons in the photoemission process. But also in that case many-particle correlations cannot be disregarded entirely. They arise in the scattering of the final state electrons, leading to losses which are roughly described by an optical potential. Including a non-hermitian potential within the hamiltonian yields Bloch vectors with complex components perpendicular to the surface plane which allow momentum non-conserving transitions with respect to that direction. These non direct transitions arise already through the presence of the surface, because the full set of states of a half-space solid incorporates states lying within the energy gaps being excluded for real Bloch vectors. The optical potential must be derived from the selfenergy describing the many-body interaction. It can be only approximately achieved from a theoretical point of view. Practically, valuable information on the optical potential can be drawn from experiment by interpreting target-current spectra. [11, 12]These spectra arise as a by-product when inverse photoemission data are collected. The incident electrons are predominantly reflected, if their energy falls into a large gap. Thus, the gap shows itself as a strong decrease in the target current whereas the band edges can be related to extrema in the first derivative of the current. The numerical analysis of those spectra follows the LEED analysis, however, at respectively very low energies as long as sharp structures from inelastic processes are supposed to be absent. In many cases that assumption proved to be justified. By comparison of theoretical with experimental spectra the optical potential can be fixed with the knowledge of a reasonable functional dependence on energy. The latter is usually represented by a monotonically decreasing function of energy for the imaginary part with a strong drop at the plasmon frequency and by a constant for the real part. The actual shape may be more complicated and is a matter of current research.

If many-particle effects have to be included the platform of the one-step model is left. Generally speaking, the photoemission process is represented by a vertex in perturbation theory which may be principally treated within arbitrary order. The golden rule expression is the lowest approximation to that expansion. Of course, the choice of an inverse LEED-state for the final state may be already seen as a kind of renormalization, i.e. a summation of diagrams representing some losses of the escaping electron. Apart from those extrinsic also intrinsic losses arise in the photoexcitation process. Their separation is a difficult task and leads to a generalization of the actual one-step model. In addition, the dielectric response to the incident photon has been shown to be important when the frequency approaches the plasma frequency. The response of lattice electrons generates local fields which are further modified by the presence of a surface. Even for the long wavelength photons of say 1000 Å the length scale of the lattice modulates the electromagnetic field. Thus, the dipole approximation used in the one-step model is no longer valid for calculating the excitation.

In the following, examples for the use of the one-step model in explaining photoemission data will be discussed. I will first concentrate on the interpretation of spectra and show also a counter example where misuse of simple band mapping methods may arise by applying them in the environment of the highest scale of resolution. Topological properties of the emission current are considered in the subsequent section. Azimuthal scans for GaAs and full $2\pi$-hemisphere patterns for Si are discussed. The effect of circular dichroism is investigated for the latter example. Another section is devoted to the screening of the photon field which in fact has to be considered in the physical photoemission process. Based on the two-dimensional behaviour layered systems represent an excellent example. I will close with a discussion of the optical potential and the selfenergy. Our latest results related to that topic appear in the framework of the GW-approximation.

## 2. Photoemission from Semiconductor Surfaces

Within the one-step model the photocurrent is calculated via

$$I \propto \; Im \sum_{i,j} \; < \Phi^{\star}_{LD}(E, \mathbf{k}_{||}) \mid \mathbf{O} \mid \psi_i > G_{ij}(E - \hbar\omega, \mathbf{k}_{||}) < \psi_j \mid \mathbf{O} \mid \Phi^{\star}_{LD}(E, \mathbf{k}_{||}) >$$

with $G_{ij}$ as the halfspace Green function of the valence states in a layer orbital LCAO basis $(i, j)$. The vector potential $\mathbf{A}$ in $\mathbf{O} = \mathbf{A} \cdot \mathbf{p} + \mathbf{p} \cdot \mathbf{A}$ is taken as a constant in the dipole approximation according to the long wavelength of the incident light. The reliability of this assumption will be discussed in section 4. The final state $\Phi^{\star}_{LD}$ corresponds to the time inverse LEED state for the outgoing electron. It is constructed from the complex band structure of a pseudopotential representation inside the crystal. The surface may be a reconstructed one in the general case which has to be regarded in the calculation of the Green function for the valence states. For the final states the solid is terminated by a solid-vacuum barrier potential which consists of a series of steps to account for the local work function of different adsorbate layers in the pseudopotential scheme. We developed a multigrid procedure to solve the Schrödinger equation with outgoing state asymptotics for an arbitrary potential in direct space. The examples cited in this section, however, were obtained with final state wavefunctions from matching the solutions at the various interfaces. The matrix elements are integrated in direct space via good lattice points. This offers a fast computation scheme in the case that the vector potential or the surface potential for the final states are position dependent and locally perturb the bulk symmetry at the surface.

The failing of band mapping methods as usually applied by deconvolution of the experimental spectra in order to get the band structure is discussed on a purely theoretical example. It yields an approximate bound below that the energy resolution cannot be fully utilized without considering the complete intensity distribution of the emitted current. A theoretical spectrum has been generated and further treated as if it would represent experimental data, i.e. standard deconvolution procedures have been applied to extract the peak positions which are then associated with corresponding levels of the bulk and surface band structure, see Fig. 1. The comparison with the electronic structure that initially was used to calculate the considered photoemission spectrum shows the error involved as a difference in the corresponding energies. Thus, experimental interpretation methods are applied to a theoretical spectrum for which the basing energy structure is already known. The ideal Ga terminated GaAs(001) surface has been chosen for that comparison. The conclusion derived from Fig. 1 will be true irrespective of the physical relevance of the surface structure which is much more complicated in reality. In the displayed spectrum a strong discrepancy between the positions marked at the true band-structure energies and at

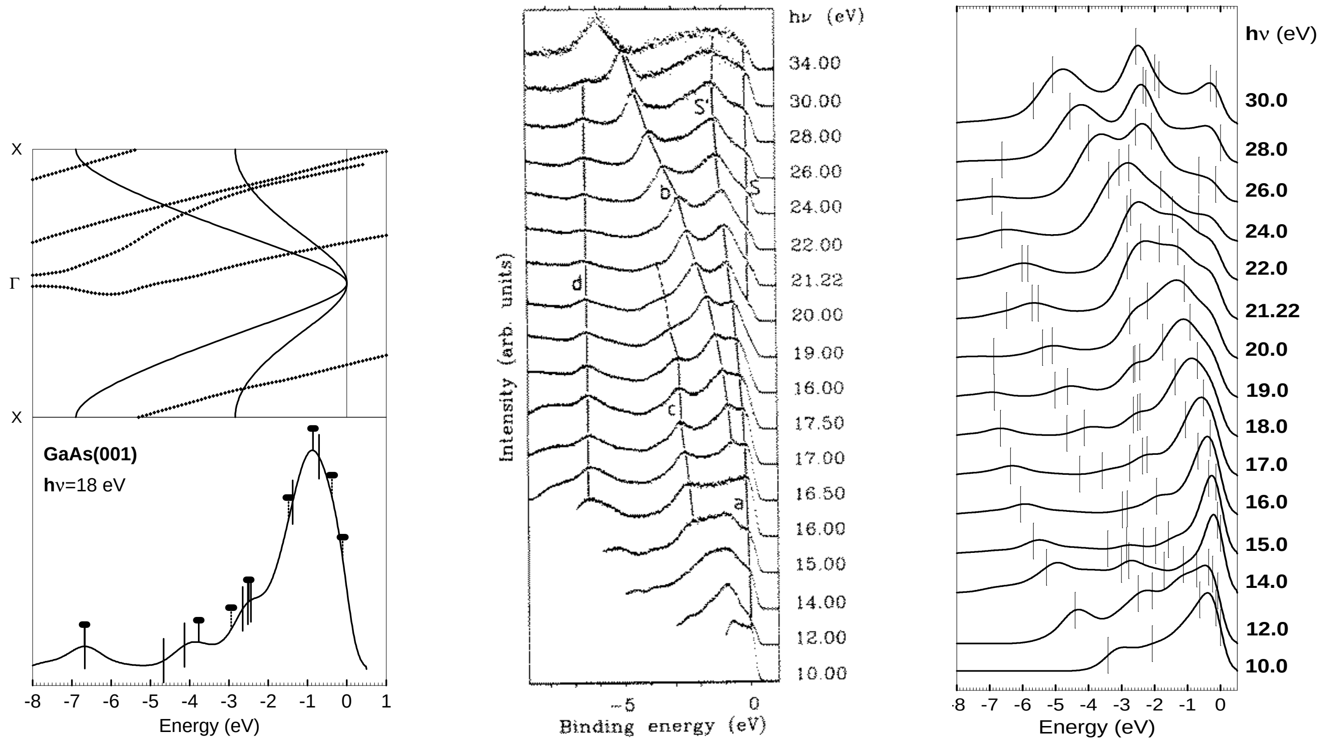


Figure 1: Left panel: Theoretical photocurrent vs. binding energy, lower part, and conduction bands shifted by the photon energy of 18 eV onto the valence bands, upper part. Filled ovals mark the experimentally deconvoluted positions, vertical bars crossing the curve denote the theoretical valence-band energies as depicted by the intersections of the two sets of bands in the upper part. Middle and right panel: A series of normal-emission experimental (middle) and theoretical (right) EDC's from the GaAs(001) surface for various photon frequencies. As a guide to the eye the dispersion is sketched by lines in experiment. The vertical bars in theory denote the valence-band energies the direct emissions start from.

the experimentally deconvoluted peaks is observed. The disagreement attains values of about 200 meV – see especially the absolute maximum near -1 eV – which clearly is not tolerable if experimental resolution lies significantly below 100 meV as it is often claimed. A series of further spectra not shown here support the finding that a reliable interpretation of photoemission data requires a combined analysis of experimental and theoretical spectra taken on the same system.

A comparison of a series of theoretical energy distribution curves (EDC) for the ideal GaAs(001) surface with experimental spectra [13] taken for the c(4x4) surface is plotted in the right panel of Fig. 1 for normal emission. The agreement is astonishingly good. In spite of the apparently different structures of the two surfaces the spectra agree in dispersion to a high degree. Parts of the deviation may be understood, because theory underestimates the damping of the final states, see section 5. It seems that the presence of terraces and other perturbations of the physical surface leads to a mixture and an averaging out of the surface properties so the bulk structure remains.

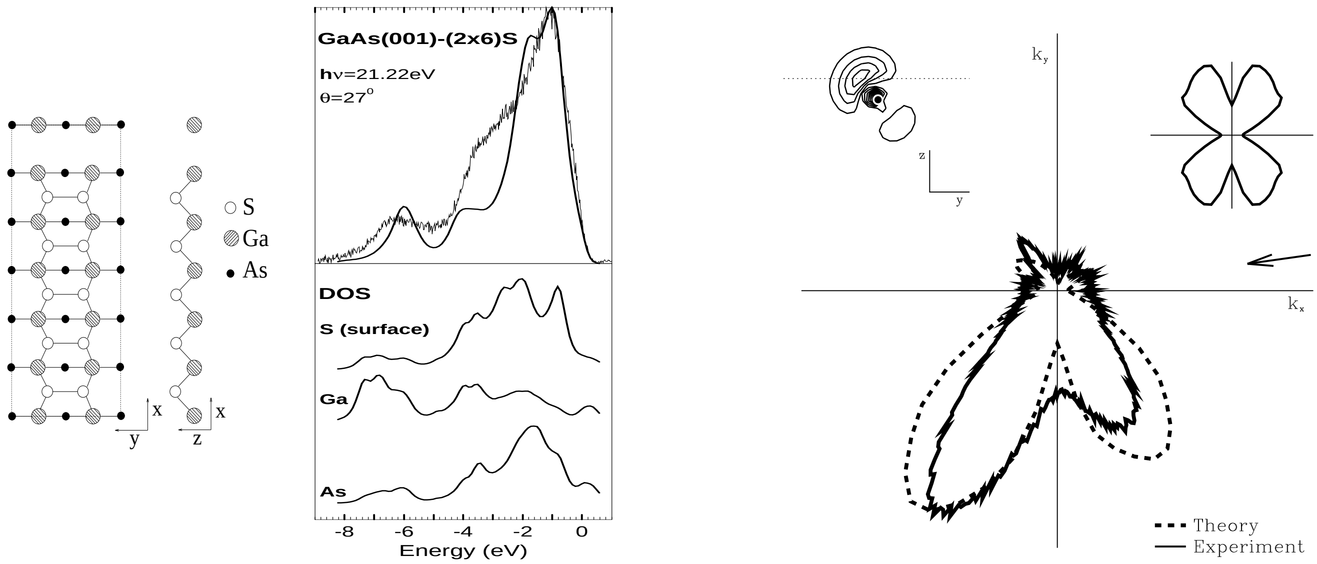


Figure 2: Left panel: Photocurrent of a special 2x6 S-dimer reconstruction as displayed at the left of the figure for an emission polar angle of 27° along the $x$-axis. The smooth curve is the theoretical result, experiment by courtesy of M. Skibowski [16]. The lower part shows the 2D-DOS at that angle, layer resolved in the sequence of their appearance from the top ( S ) to the interior. Right panel: Theoretical azimuthal scan of the photocurrent from GaAs(110), broken line. Experiment, solid line, was made available by courtesy of M. Skibowski [17]. The distance from zero characterizes the normalized photocurrent. The incident light direction is marked by the arrow. Left upper insert shows the dangling-bond density with respect to the $(y, z)$-axes below, right upper insert displays the 2D-DOS in the $(k_x, k_y)$-coordinate frame.

This agrees with the finding that most of the peaks can be attributed to bulk emissions. [13]

The GaAs(001) surface can be converted into a more stable one by passivation with sulphur, though types of the reconstructions under specific growing conditions are not fully known. A 2x3 reconstruction, maybe 2x6, was observed in Skibowski's group, where photoemission spectra have been measured, but geometric data for the positions are not available. Of course, a LEED investigation or molecular dynamics calculation can resolve the problem. The 1x1 coverage with one monolayer sulphur already was treated within molecular dynamics. [14] We evaluated photoemission spectra for a bunch of structures allowed by chemical arguments and discarded those with a strong disagreement between the respective photocurrents. The bulk seems to be most probably Ga terminated, covered by a monolayer of a mixture of S and As atoms. The arrangement of the adatoms was varied and, as to be expected, did not reveal differences which could be decisive for the selection of a special structure. A typical example is shown in the left panel of Fig. 2 with a 2x6 reconstruction displaying how experiment and theory are still at variance. This model was suggested by STM investigations. [15] A sequence of five parallel S-dimers on the underlying Ga surface was assumed. Surely, the photoemission investigation is not thought to replace a structural analysis. It might add complementary geometrical information, but it reveals the orbital composition and the binding mechanism reflected by the energetic structure. In the case here considered, a prominent structure arises between 0 and 3 eV to be attributed to the sulphur overlayer with peaks in the density of states (DOS) at about -0.8 and -2.2 eV. The shoulder around -4 eV coincides with peaks of the DOS of both Ga and S. Also the step at -7 eV is related to these elements displaying a double peak of the DOS. The overall structure of the spectra suggests that the dominant influence results from the sulphur overlayer whereas the layers below add a minor contribution to the photocurrent. This is in contrast to the pure GaAs(001) surface where mainly bulk features are observed. [13] Of course, in all cases only the first few layers establish the photocurrent, and bulk features arise by the presence of their wavefunction in that region only. In concluding this section it is thus stated that in spite of the surface sensitivity of photoemission bulk electronic properties can be detected by a spectral representation, especially with normal-emission spectra. This is opposed to the point of view taken in the next section.

## 3. Interpretation of Two-dimensional Patterns

Two-dimensional representations of photoemission data are used quite commonly in core-level and very rarely in valence-band spectroscopy. The inclusion of the valence bands within the photoemission calculation adds the difficulties of band-structure determinations to the scattering calculations of the final-states if viewed from the theoretical point. The one-step model takes advantage from the two-dimensional translational lattice symmetry whereas the photoelectron diffraction is determined within a cluster scattering scheme, yielding two very different numerical approaches. Nevertheless, rising computer power brought the breakthrough also for the valence-band photoemission. Experimentally, recent developments in detector design favour the collection of two-dimensional patterns. The energy resolution does not compare with the traditional scanning methods at the moment, however, it is increasing and it seems not to be as important for pattern interpretation as for the discussion of spectra.

The numerical procedure follows the path of the one-step model. At the comparably low frequencies of the vacuum-ultraviolet photon regime the anisotropy of the crystal potential has to be observed. The calculation of the final states requires the overwhelming amount of computer resources, CPU time as well as storage capacity. With the help of an LCAO parametrization the initial-states Green function can be computed very fast, whereas the outgoing inverse LEED states are gained by a matching procedure in a plane wave basis, separately for each angle and each energy. The calculational scheme allows a separation of the Green-function influence, i.e. essentially the two-dimensionally resolved density of state (2D-DOS), from the effect of the final states. The latter include the transition matrix elements and establish a connection to an interpretation in terms of the photoelectron diffraction. Both contributions which are expanded in a layer-orbital basis constitute the photocurrent as a sum of direct diagonal parts and, additionally, of nondiagonal parts. Because of interference the latter usually do not admit a simple description.

Figure 2 right panel displays experimental and theoretical data on an azimuthal scan of emissions from the dangling bond of the GaAs(110) surface. The plot also shows the 2D-DOS exhibiting two mirror planes, one along the $k_y$-axis arising from crystal symmetry and a second one along the $k_x$-axis associated with Kramer's degeneracy. Both symmetries are broken in the photoemission scan by the effect of matrix elements and final states. The mirror plane along $y$ gets changed by the incidence direction of the light thereby strengthening the emissions being in line with that direction. Kramer's degeneracy is absent in the three-dimensional system with current-carrying damped states, and the asymmetry of the dangling bond with respect to the mirror, $y \rightarrow -y$, strongly alters the pattern. The overwhelming emission is found into the direction of the dangling bond. The entire polar diagram seems to show the geometrical arrangement of the dangling-bond charge density modulated by the 2D-DOS. The agreement between theory and experiment is excellent, especially if one compares with the agreement usually attained for EDC's.

The generalization of the azimuthal scans to a full hemisphere representation is seen in Fig. 3 for the ideal Si(001) surface. Circular dichroism being associated with chirality of a system may also serve as a probe for surface structures, especially for adsorbed molecules. [18] Recent investigations observed non-magnetic circular dichroism in core level photoemission patterns. [19, 20] A rotation of the emission spots according to the angular momentum of the initial core level and that of the incident photon could be explained by a lucid quantum mechanical argument using angular momentum conservation and forward scattering at high kinetic energies. Because the different orbital momenta are superimposed in the valence states and forward scattering is not thus dominant in the vacuum ultraviolet photon regime one cannot expect to find a unique rotation in proceeding from left to right circularly polarized light. However, there are cases as it is shown in Fig. 3, left panel, where this rotation might be observed. The bright spots clearly move clockwise if polarization is changed from left to right. This results from an analogous behaviour of the matrix elements in the middle panel. The forward scattering may be attributed to $p_x$-hybrids along the chain directions, see upper right panel of Fig. 3. Comparing with the 2D-DOS, major intensity arises from two bright regions on a line parallel to the $k_x$-axis in the middle between two

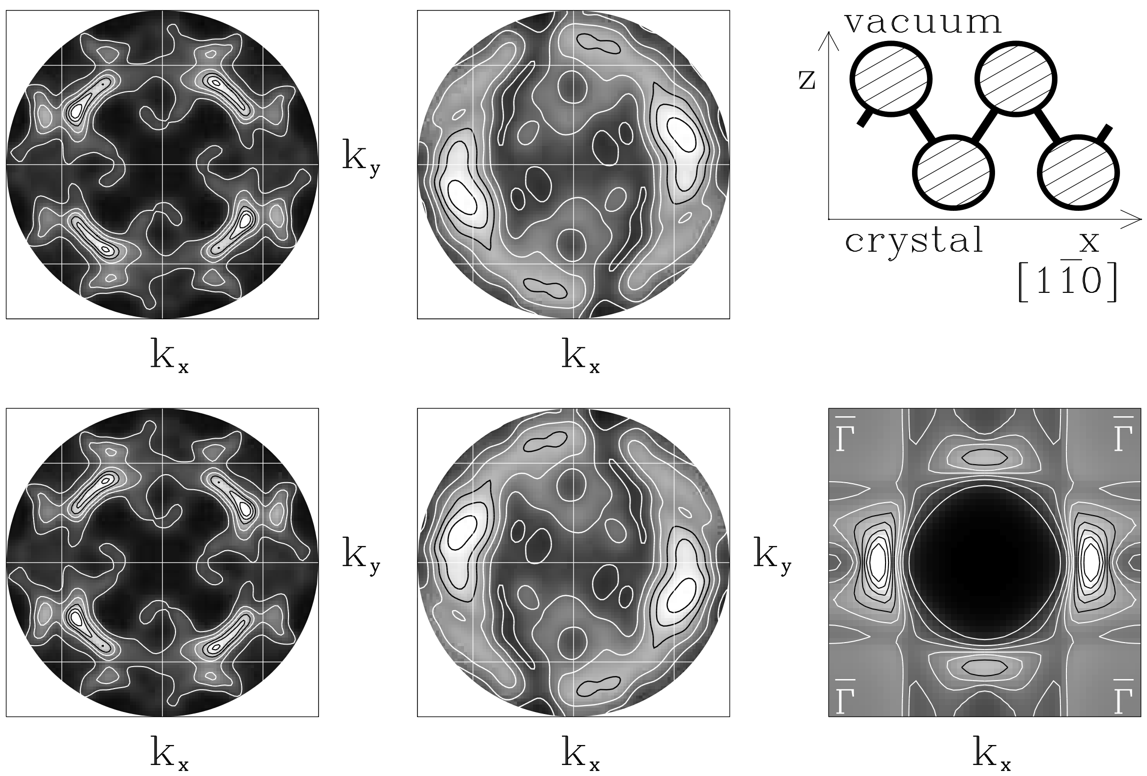


Figure 3: Left panel and middle panel show the photocurrent and for the first four planes from the surface the $p_x$-matrix element, resp., over the full $2\pi$-hemisphere for ideal Si(001) at normal incidence of left (right) circularly polarized light in the upper (lower) part. The grey scale associates white with the maximum. The net denotes the reciprocal lattice with each square mesh extending over the two-dimensional Brillouin zone which is displayed in the lower part of the right panel with the 2D-DOS of the first two layers. The latter are depicted in the upper part to define the axes relative to the uppermost bonding chains. Valence band energies are collected from -2.2 to -1.8 eV covering a surface state with mainly $p_x$-character. The final state energy is 30 eV above valence band maximum.

$\Gamma$-points and with a smaller amount on the respective orthogonal direction. Normal emission is extinguished because of the symmetry for normal incident light so the center of the emission pattern remains dark. Altogether, the intensity generally arises from high 2D-DOS regions weighted by the matrix elements though interference between different orbitals may change the simple picture.

To summarize, the two-dimensional representation of the photocurrent yields the surface parallel electronic structure as far as it is localized in a narrow surface sheet, i.e. the detection is much more localized than in the case of the interpretation of normal emission spectra. The theoretical intensity varies over orders of magnitudes within one pattern and the main structures are surface determined ones. In the case of spectral representations one often encounters low intensity situations which then reveal bulk features because they are not surface dominated. Apart from this, the valence electronic surface topology appears in the two-dimensional patterns. The separate numerical investigation of the final state with inclusion of the matrix elements projected onto an atomic orbital basis bridges the gap to photoelectron diffraction.

## 4. Screening of the Photon Field

Extending the one-step model beyond the dipole approximation for the external field changes the operator $\mathbf{O} = \mathbf{p} \cdot \mathbf{A} + \mathbf{A} \cdot \mathbf{p}$ to incorporate a position dependent vector potential instead of the constant one. The final states of this section have been calculated with a pseudopotential together with an expansion into plane waves, and for comparison, also through the layer KKR method with muffin-tin potentials. The main problem to be solved is the construction of a suitable vector potential. This goes far beyond the application of text book optics of using Fresnel's formulae. In the best case one would have to calculate selfconsistently the surface response of the solid to an external electromagnetic field. This is a formidable task and has not yet been achieved for a realistic system. There is a long history in the treatment of a jellium surface and a new interest [21, 22] in the effect of crystallinity upon the surface response. A one-dimensional modelling of that crystallinity led to the result that the well known multipole plasmon evolving at a jellium surface is essentially suppressed by a covalent bonding of the available electronic charges in the solid. The original idea thought this resonance to be responsible for an observed photoemission enhancement in layered crystals. In a normal emission experiment on layered dichalcogenides the dispersing states of the interlayer coupling orbitals show an enhanced current compared with the in-plane states. It could be understood if an additional longitudinal field pointing along the surface normal, as it is observed in the jellium case, couples to the perpendicularly directed orbitals. Those fields proved to be not strong enough to explain the experimental results for frequencies below the plasma frequency. Instead, it was found in the one-dimensional model that bulk local fields may lead to a more important enhancement in the vicinity of the plasma frequency. The induced local fields are obtained via an inversion of the frequency dependent dielectric matrix with respect to the reciprocal lattice vectors of the crystal. As an example, Fig. 4 displays for $TiSe_2$ the first two elements of the inverse dielectric matrix showing strong structures around the plasma frequency of $\hbar\omega = 19.6$ eV. This behaviour leads to local field contributions proportional to the magnitude of the matrix element and with wavelengths related to the considered reciprocal lattice vectors. These induced fields pointing parallel to the layer normal are supposed to couple in photoemission appreciably to orbitals with the same preferential direction. The layer parallel

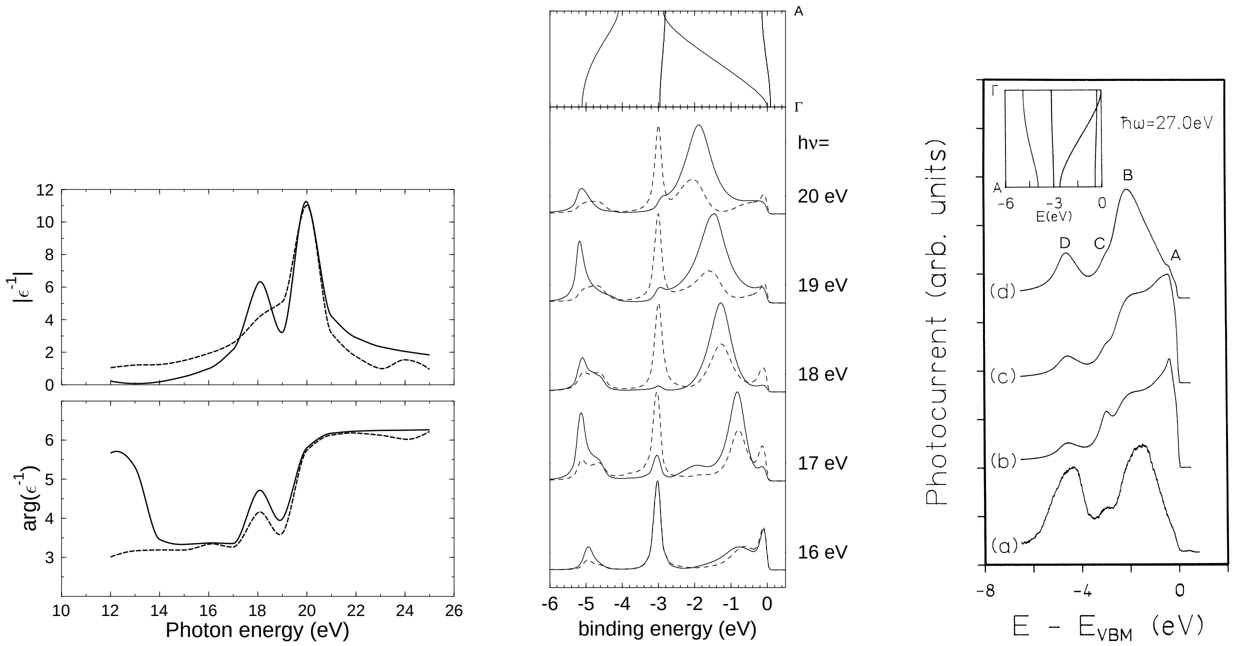


Figure 4: Left panel: Modulus (upper part) and phase (lower part) of the inverse dielectric function components $\epsilon^{-1}_{zz}(\mathbf{0},\mathbf{0};\omega)$ and $\epsilon^{-1}_{zz}(\frac{2\pi}{c}\mathbf{e}_z,\mathbf{0};\omega)$ plotted vs. frequency as solid and broken line, respectively. [25] The modulus shown by the broken line has been augmented by a factor of 5. Middle panel: Photocurrent vs. initial state energy of normal emission spectra for photon frequencies as indicated at the curves with incidence angle of 45°. The screening of the photon yields the solid lines as opposed to the unscreened result depicted by the broken lines. The upper panel shows the respective part of the bandstructure. Right panel: Normal emission photocurrent from $TiS_2(001)$ for photon energy $\hbar\omega = 27.0$ eV above the plasma frequency of $\hbar\omega_p = 21.5$ eV is plotted, (a) from experiment and (b),(c),(d) from theory; (b) for unchanged incident light, (c) for refracted light using Fresnel's formulae, (d) for the hydrodynamic model as the surface screening mechanism. [26] The insert shows the bandstructure along the associated Γ-A direction. The peak labels A, B, C, and D are referred to the emitting initial bands counted from top to bottom. Notice peak B and D which belong to dispersive bands with large $p_z$-orbital character. Using the hydrodynamic model significantly improves the agreement with experiment owing to the increased current from the dispersive bands.

dielectric matrix does not exhibit such an anomalous behaviour. The resulting normal emission spectra are shown in Fig. 4 for a set of frequencies below and near the plasma frequency. The induced local fields pronounce the current from both dispersive bands between 17 and 20 eV photon energy in such an essential way that even peak positions appear to be shifted by more than 100 meV in comparison to the spectra with the unscreened fields.

For photon energies above the plasma frequency also the surface response may yield a considerable enhancement of the emission current from the dispersive orbitals as it was shown through modelling the response via the hydrodynamic equations with suitable boundary conditions. Different from the multipole mode below $\omega_p$ virtual longitudinal plasmons couple to the layer perpendicular orbitals above $\omega_p$, see Fig. 4. The result of the hydrodynamic model compares well with experiment whereas the agreement is poor for both using the unperturbed light or applying the refracted light. Even if the correct screening model may be subject to discussion, the calculation proves that drastic changes occur by the electronic response to the incident light being due to virtual excitation of plasmons.

## 5. Optical Potential and Selfenergy

In order to take into account many particle effects in photoelectron spectroscopy, selfenergy corrections have to be considered in the one-particle Green function and corrections have to be applied to the photoemission vertex. Contributions from electron-electron interactions are included in the complex selfenergy $\Sigma$ being added to the one-particle energy in the non-interacting Green function

$$G(E) = \frac{1}{E - H - \Sigma(E)}$$

The real part of the selfenergy describing the elastic scattering shifts the energy levels whereas the imaginary part reflecting the losses gives an exponential damping of the wave function amplitude. Vertex corrections are omitted in this section.

Because of the finite lifetime of the escaping photoelectron, photoemission is a surface sensitive experiment. Electrons produced far away from the crystal surface cannot reach the surface and will not contribute to the photocurrent. Therefore the outgoing states in photoemission are localized near the crystal surface and damped inside the crystal. In terms of LEED the selfenergy usually is denoted as an optical potential. The following heuristic formula for this damping has shown its usefulness in many calculations of photoemission spectra[9, 23, 24]

$$\mathrm{Im}\,\Sigma(E) = \frac{a}{1 + \exp(-(E - \omega_p)/c)} + d$$

The shape of this function shows a strong increase in absolute magnitude above the plasma frequency $\omega_p$ associated with plasmon excitations. A typical set of parameter values,($a = -2.4, d = -0.3, c = 1.8$, all in eV), is taken from the case of layered dichalcogenides. This set which leads to values varying from -0.3 eV at about 10 eV photon frequency to -2.7 eV above the plasma frequency has to be compared with the values obtained for $TiTe_2$ ($\omega_p$ = 18 eV) from a more fundamental investigation within this section.

Much of our present knowledge about the selfenergy is based on GW calculations[27], i.e. vertex corrections being neglected in the perturbation expansion

$$\Sigma(\vec{r}, \vec{r}\,', E) = \frac{i}{2\pi} \int dE'\; e^{iE'\delta}\; G(\vec{r}, \vec{r}\,', E + E')\; W(\vec{r}, \vec{r}\,', E')$$

This formula requires the knowledge of the Green function and the dynamically screened interaction $W = \epsilon^{-1}V$. Here, we consider the dielectric matrix as being diagonal because only its frequency dependence is available for $TiTe_2$

$$\epsilon^{-1}_{\vec{G}\vec{G}'}(\vec{k}, E) \quad = \quad \epsilon^{-1}(E) \cdot \frac{(\vec{k}+\vec{G})^2}{(\vec{k}+\vec{G})^2 + \kappa_{TF}^2} \, \delta_{\vec{G}\vec{G}'}$$

To account for the long wavelength screening a Thomas-Fermi cut-off with $\kappa_{TF} = 1.55\text{Å}^{-1}$ has been used. Finally, the following expression for a diagonal matrix element of the selfenergy matrix is obtained.

$$\Sigma_{\vec{G}_1\vec{G}_2}(\Gamma, E) = \frac{i}{(2\pi)^4} \sum_{\vec{G}'} \int_{BZ} d\vec{k}' \int dE' \; e^{iE'\delta} G_{\vec{G}'\vec{G}'+\vec{G}_2-\vec{G}_1}(\vec{k}', E+E') \, W_{\vec{G}_1-\vec{G}',\vec{G}_1-\vec{G}'}(-\vec{k}', E')$$

Only the $\vec{k} = 0$ contribution, i.e. that at the $\Gamma$–point, is taken into consideration because for simplicity it will be applied to a quasi-local crystal potential, the same potential which is also used to evaluate the Green function.

For illustration the shape of the diagonal matrix element for $\vec{G} = (0, 0, 0)$ is shown in Fig. 5. The other diagonal elements are slowly decreasing with $\vec{G}$. As to be expected from the homo-

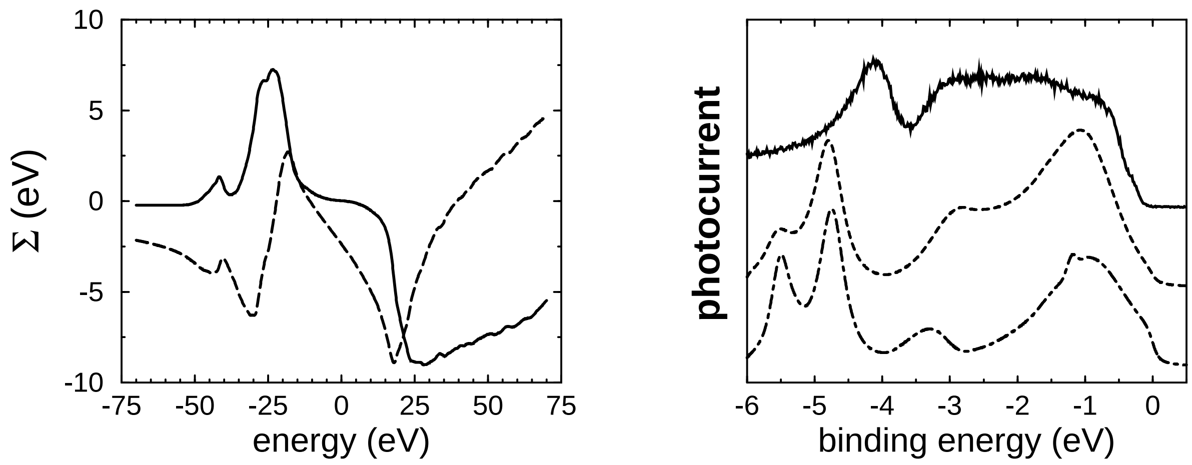


Figure 5: Left panel: Real (dashed line) and imaginary part (solid line) of the GW selfenergy matrix element $\Sigma_{\vec{G}\vec{G}}$ of $TiTe_2$ belonging to $\vec{G} = (0, 0, 0)$. The real part has been shifted by the Hartree-Fock part $-\Sigma^{HF} = 6.1$ eV. Right panel: Photocurrent vs. initial state energy of normal emission spectra for a photon frequency of 20 eV with an incidence angle of 45°. Using the calculated imaginary part of the selfenergy yields the dashed curve whereas the heuristic damping leads to the dot-dashed line. The experimental spectrum is displayed as a solid line. [28]

geneous electron gas, the imaginary part becomes small near the zero of energy (Fermi level).

It essentially rises in magnitude at $\pm\omega_p$ and attains twice the value suggested by the heuristic formula for the optical potential.

The obtained selfenergy was applied to determine emission spectra for $TiTe_2$, see Fig. 5 This material has attracted much attention in view of the detection of a Fermi liquid, because an isolated photoemission peak could be clearly followed through the Brillouin zone as it was crossing the Fermi level in non-normal emission. [29] For the corresponding photoemission calculation see reference [30]. Here, only normal emission is considered. Obviously, the position of the calculated gap at -4 eV deviates from experiment, a weakness of the band-structure determination. However, in contrast to the heuristic damping the use of the calculated selfenergy improves the spectra for large as well as smaller binding energies. In the first case the peak at -5.5 eV is suppressed by the increasing imaginary part of the selfenergy below the Fermi level affecting the initial-states' calculation, in the second the intensity is increased between -3 eV and -1 eV attributed to the increased damping of the final states at this photon frequency. The latter may be seen as caused by additional indirect transitions which do not conserve the surface perpendicular momentum.

The presented results on the selfenergy show that the optical potential, i.e. the escape depth which generally is known only empirically, may be determined in practice from first principles.

## Acknowledgements

The author appreciates with thanks the calculations and drawings of T. Strasser on the GaAs(001) spectra, of C.-H. Solterbeck on two-dimensional photoemission, of A. Bödicker on the selfenergy topic, and of Dr. E.E. Krasovskii on the $TiTe_2$ dielectric function. He is indebted to Prof. M. Skibowski and his experimental group for continuous collaboration and Prof. C.S. Fadley for suggesting investigations on the two-dimensional valence-band photoemission. The work was substantially supported by the Deutsche Forschungsgemeinschaft and by the Bundesministerium für Bildung, Wissenschaft, Forschung und Technologie.

## References

# References

[1] J. Henk and R. Feder, *Europhys. Lett.* **28**, 609 (1994); R. Feder and J. Henk, in *Spin-Orbit Influenced Spectroscopies of Magnetic Solids*, H. Ebert, G. Schuetz, (Eds.), Lecture Notes in Physics, Springer, Berlin (1995); J. Henk, T. Scheunemann, S. V. Halilov, and R. Feder, *J.*

*Phys.: Condens. Matter* **8**, 47 (1996).

[2] G. Schönhense, *Physica Scripta* **T31**, 255 (1990).

[3] H. Nishimoto, H. Daimon, S. Suga, Y. Tezuka, S. Ino, I. Kato, F. Zenitani, and H. Soezima, *Rev. Sci. Instrum.* **64**, 2857 (1993).

[4] A. Santoni, L.J. Terminello, F.J. Himpsel, and T. Takahashi, *Appl. Phys.* A **52**, 299 (1991).

[5] P. Aebi, J. Osterwalder, P. Schwaller, L. Schlapbach, M. Shimoda, T. Mochiku, and K. Kadowaki, *Phys. Rev. Letters* **72**, 2757 (1994).

[6] H. Daimon, *Rev. Sci. Instrum.* **59**, 545 (1988)

[7] C.S. Fadley, *Surf. Sci. Repts.* **19**, 231 (1993)

[8] C.-H. Solterbeck, W. Schattke, and C.S. Fadley, *Surf. Sci.* (1996) in press.

[9] J. Henk, W. Schattke, H. Carstensen, R. Manzke, and M. Skibowski, *Phys. Rev.* B **47**, 2251 (1993).

[10] M. Graß, J. Braun, and G. Borstel, *J. Phys.: Condens. Matter* **7**, 7775 (1995); *Prog. Surf. Sci.* **46**, 107 (1994).

[11] J.V. Peetz, W. Schattke, H. Carstensen, R. Manzke, and M. Skibowski, *Phys. Rev.* B **46**, 10127 (1992).

[12] V.N. Strocov and H.I. Starnberg, *Phys. Rev.* B **52**, 8759 (1995).

[13] J. Olde, G. Mante, H.P. Barnscheidt, L. Kipp, J.C. Kuhr, R.Manzke, M.Skibowski, J.Henk, and W. Schattke, *Phys. Rev.* B **41**, 9958 (1990).

[14] T. Ohno and K. Shiraishi, *Phys. Rev.* B **42**, 11194 (1990); T. Ohno, *Surf. Sci.* **255**, 229 (1991).

[15] S. Tsukamoto, N. Koguchi, *Appl. Phys. Letters* **65**, 2199 (1994).

[16] K. Gohrt, Diploma thesis, Kiel (1996); T. Strasser, A. Bödicker, C. Solterbeck, W. Schattke, K. Gohrt, R. Schnurpfeil, L. Kipp, and M. Skibowski, *Verhandl. DPG* (VI) **31**, 1906 (1996).

[17] J.-W. Zahlmann-Nowitzki, Diploma thesis, Kiel (1996); J.-W. Zahlmann-Nowitzki, K.-U. Gawlik, S. Harm, K. Behnke, L. Kipp, M. Skibowski, C. Solterbeck, and W. Schattke, *Verhandl. DPG* (VI) **31**, 1845 (1996).

[18] C. Westphal, J. Bansmann, M. Getzlaff, and G. Schönhense, *Phys. Rev, Letters* **63**, 151 (1989).

[19] H. Daimon, T. Nakatani, S. Imada, S. Suga, J. Kagoshima, and T. Miyahara, *Jpn. J. Apl. Phys.* **32**, L1480 (1993).

[20] A.P. Kaduwela, H. Xiao, S. Thevuthasan, C.S. Fadley, and M.A. van Hove, *Phys. Rev.* B **52**, 14922 (1995).

[21] J.T. Lee and W.L. Schaich, *Phys. Rev.* B **43**, 4629 (1991); K. Burke and W.L. Schaich, *Phys. Rev.* B **49**, 11397 (1994).

[22] D. Samuelsen and W. Schattke, *Phys. Rev.* B **51**, 2537 (1995); *Surf. Sci.* **327**, 379 (1995).

[23] T. Grandke, L. Ley, and M. Cardona, *Phys. Rev.* B **18**, 3847 (1978).

[24] E. Pehlke, W. Schattke, O. Anderson, R. Manzke, and M. Skibowski, *Phys. Rev.* B **41**, 2982 (1990).

[25] A. Bödicker, A. Leventi-Peetz, W. Schattke, *J. Electron Spectrosc. & Relat. Phenom.* (1996) in press

[26] D.Samuelsen, E.Pehlke, W.Schattke, O.Anderson, R.Manzke, M.Skibowski, *Phys. Rev. Letters* **68**, 522 (1992)

[27] L. Hedin and S. Lundquist, *Solid State Physics* **23**, 1 (1969).

[28] S. Harm, PhD Thesis, Kiel, (1994).

[29] R. Claessen, R. O. Anderson, J. W. Allen, C. G. Olson, C. Janowitz, W. P. Ellis, S. Harm, M. Kalning, R. Manzke, and M. Skibowski, *Phys. Rev. Lett.* **69**, 808 (1992); S. Harm, R. Dürig, R. Manzke, M. Skibowski, R. Claessen, and J.W. Allen, *J. Electron. Spectrosc. & Relat. Phenom.* **68**, 111 (1994).

[30] A. Bödicker, W. Schattke, *J. Electron Spectrosc. & Relat. Phenom.* **76**, 265 (1995).